Extended Time Varying Multi-Cluster Fluctuating Two-Ray Fading Model for Maritime Environment

Antoine Thibault Vié* Roberto Galeazzi*
Dimitrios Papagergiou*

* Electrical Engineering Department, Technical University of Denmark, Kas. Lungby, Danemark, (e-mail: author@dtu.dk)

Abstract: The recent advancements in autonomous and remote operation of maritime vessels necessitates the development of robust and reliable communication systems to support high-bandwidth applications such as real-time monitoring, navigation, and control. Existing communication channel models, including Rayleigh and Rician fading, are inadequate to accurately describe the dynamic and complex nature of maritime communication, particularly for high-speed vessels in coastal environments. This paper proposes an extension to the Multi-Cluster Fluctuating Two-Ray Fading (MFTR) model that also accounts for key phenomena such as large-scale fading, time-varying parameters and Doppler shifts. The extended MFTR model integrates Stochastic Differential Equations (SDEs) to capture the time-varying characteristics of the channel, such as phase shifts and delays, while considering physical factors like delayinduced power loss and path loss. The accuracy of the proposed model is assessed in simulation.

Keywords: Marine system identification and modeling, Wireless communication, Time-varying systems, Stochastic hybrid systems, Systems with time delays

1. INTRODUCTION

The maritime industry has experienced significant growth in recent years, driven by increased global trade. The growing need for efficient and sustainable transportation solutions has heightened the interest in autonomous and remotely-piloted vessels, which promise to revolutionize maritime operations by improving safety and resilience. This shift towards high levels of automation necessitates robust and reliable communication systems capable of supporting high-bandwidth applications, such as real-time monitoring, navigation, and control of autonomous ships. Consequently, there is an increasing demand for higher data rates and more efficient communication technologies to ensure seamless connectivity in maritime environments.

For near-coast maritime operations, 4G and 5G technologies are emerging as the backbone of communication systems, offering the necessary high-speed data transfer capabilities. However, classical channel models, such as Rayleigh and Rician fading models (Tse and Viswanath, 2005), which have been widely used in wireless communication systems, are often insufficient to accurately model the dynamic and complex nature of maritime communication (Wang et al., 2018), particularly in the context of high-speed vessel operation and harsh propagation environments.

The advancements in the use of 4G and 5G wireless technologies require more sophisticated models to address the unique challenges posed by maritime environments (Wang et al., 2018), (Romero-Jerez et al., 2017), (Hemadeh et al., 2018), (Marins et al., 2021), (Eggers et al., 2019).

In recent years, several new models have emerged that offer more accurate and flexible representations of the channel. Notably, the $\kappa-\mu$ shadowed fading distribution (Moreno-Pozas et al., 2016), the extended Round Earth Loss (REL) model (Ekman, 2024), and the Fluctuating Two-Ray (FTR) fading model (Romero-Jerez et al., 2016), have all been proposed as more accurate alternatives. Furthermore, the Multi-Cluster Fluctuating Two-Ray Fading (MFTR) model (Sánchez et al., 2024) has been introduced, reconciling the two dominant fading approaches, $\kappa-\mu$ shadowed fading and the FTR model, providing a simplified yet accurate representation of the channel.

Despite the advancements offered by these models, they fail to capture several important physical aspects of the communication channel. Specifically, they do not account for the large-scale fading characteristics, the time-varying nature of the channel, the inherent loss of power due to delays, Doppler shifts derived from Jakes' model, or the impact of distance on macro parameters. These limitations reduce their accuracy in real-world scenarios, where such factors play a critical role in system performance (Wang et al., 2018).

Addressing the shortcomings of existing models will facilitate a more comprehensive and accurate representation of the maritime communication channel, enhancing the reliability of communication systems for autonomous and remote piloted vessels in near-coast environments. To this end, the paper proposes an extension to the MFTR model that includes the aforementioned physical aspects. Specifically, this work contributes by

- Incorporating baseband modeling and an explicit representation of Doppler shifts.
- Applying Stochastic Differential Equations (SDEs) for handling time-varying parameters.
- Modeling of path loss effects arising from propagation delays.

The remainder of the paper is organized as follows. Sections 2 and 3 provide an overview of the large-scale and small-scale fading phenomena, respectively, prevalent in maritime communication dynamics, as well as existing modelling frameworks for them. Section 4 details the model extensions proposed in this work. Section 5 demonstrates the model efficacy via simulations. Finally, Section 6 provides concluding remarks.

2. NEAR SEA-SURFACE LARGE-SCALE FADING

Large-scale fading refers to the gradual variation of received signal power over distance due to path loss and shadowing. As mentioned in (Wang et al., 2018; Habib and Moh, 2019; Lee et al., 2014), various channel models have been investigated and applied in the context of maritime communication. Lee et al. (2014) demonstrated that certain models provide an accurate representation of real-world conditions. In our study, to derive a physically meaningful model, empirical models have been excluded, and only analytical models have been considered. Consequently, the simplest path loss model, known as Free Space Loss (FSL), is given by:

$$L_{FSL}(t) = \left(\frac{\lambda}{4\pi d(t)}\right)^2, \qquad (1)$$

where λ represents the signal wavelength, and d denotes the transmitter-receiver distance. This model assumes an unobstructed line-of-sight (LOS) propagation environment, as well as the absence of reflections. However, in a maritime setting, multipath propagation effects must be taken into account, for example, due to signal reflections off the sea surface and nearby vessels, which can lead to time-dispersive and frequency-selective fading. This phenomenon is particularly critical for ship-to-shore and intership communication links (Coker et al., 2013).

As described in (Wang et al., 2018), the two-ray model provides an accurate characterization within the defined range, under the assumption of an ideal reflection coefficient $\Gamma = -1$ and a distance range of $d \in \{d_0, d_{break}\}$, where d_{break} is given by:

$$d_{break} = \frac{4h_t h_r}{\lambda} \,. \tag{2}$$

The parameters h_t and h_r denote the heights of the transmitter and receiver, respectively. The corresponding path loss model is expressed as:

$$L_{2-ray}(t) = 4L_{FSL}(t)\sin\left(\frac{2\pi}{\lambda}\frac{h_t h_r}{d(t)}\right)^2.$$
 (3)

For distances exceeding the breakpoint d_{break} , the ducting effect must be considered (Lee et al., 2014). Therefore, when $d \in \{d_{break}, d_{LOS}\}$, where d_{LOS} is given by:

$$d_{LOS} = \sqrt{h_t^2 + 2h_t R} + \sqrt{h_r^2 + 2h_r R}$$
 (4)

with R representing the Earth's curvature, the three-ray model is defined as:

$$L_{3-ray} = 4L_{FSL}(t)(1+b(t))^{2}.$$
 (5)

The parameter b is given by:

$$b(t) = 2\sin\left(\frac{2\pi h_t h_r}{\lambda d(t)}\right) \sin\left(\frac{2\pi (h_e - h_r)(h_e - h_t)}{\lambda d(t)}\right)$$
 (6) with h_e representing the effective duct height. Consecutive duct height.

with h_e representing the effective duct height. Consequently, the overall large-scale fading behavior can be summarized as follows:

$$L(t) = \begin{cases} L_{FSL}(t) & \text{if } d(t) < d_0, \\ L_{2-ray}(t) & \text{if } d(t) \in \{d_0, d_{break}\}, \\ L_{3-ray}(t) & \text{if } d(t) \in \{d_{break}, d_{LOS}\} \end{cases}$$
(7)

3. SMALL-SCALE FADING

Small-scale fading arises due to rapid channel variations caused by multipath propagation and Doppler effects. In maritime environments, where reflections from the sea surface and vessel motion introduce time-selective and frequency-selective fading, accurate modeling is crucial for reliable communication.

3.1 Channel State Preliminaries

As explained in (Tse and Viswanath, 2005) the baseband multipath channel is modeled as a linear Finite Inpulse Response (FIR) and is expressed as:

$$h_b(\tau, t) = \sum_i a_i^b(t)\delta(\tau - \tau_i(t))$$
 (8)

where $a_i^b(t)$ and $\delta(\tau - \tau_i(t))$ denote amplitude of a path in the baseband and the Dirac delta function, respectively. Since the Z-transform of a delayed Dirac function is known, the channel can be written in the Z-domain as:

$$H(z;t) = \sum_{i} a_i^b(t) z^{-\tau_i(t)f_s}$$
(9)

where f_s denotes the sampling frequency. This system is a LTV system. However, as defined in (Tse and Viswanath, 2005), the channel coherence time can be determined, representing the duration between two instances where the channel can be approximated as a linear time-invariant (LTI) system. The coherence time is given by:

$$T_c = \frac{1}{4D_s} \tag{10}$$

with D_s being the Doppler spread of the channel.

3.2 The Multi-Cluster Fluctuating Two-Ray Fading Model

Romero-Jerez et al. (2017) introduced the Fluctuating Two-Ray Fading Model (FTR), and Wang et al. (2018) pointed out that it is an effective model when the distance remains below the break point. Sánchez et al. (2024) proposed an extension, which resulted in the Multi-Cluster Fluctuating Two-Ray Fading Model (MFTR), which can be applied beyond the break point by adjusting parameters when the LOS components are weaker.

The MFTR model is expressed as:

$$W = |\sqrt{\zeta} \left(V_1 e^{j\phi_1} + V_2 e^{j\phi_2} \right) + Z_1|^2 + \sum_{i}^{\mu} |\sqrt{\zeta} U_i e^{j\varphi_i} + Z_i|^2$$
(11)

where μ is the number of multipath components, U_i denotes the specular component of the i^{th} cluster, $\phi_i, \varphi_i \sim$

 $\mathcal{U}(0,2\pi)$ are uniformly distributed random variables, ζ is a unit-mean Gamma distribution with probability density function (PDF):

$$f_{\zeta}(x) = \frac{m^m x^{m-1}}{\Gamma(m)} e^{-mx} \,. \tag{12}$$

Here m denotes the shadowing severity index of the specular components. The LOS components V_1, V_2 are defined as:

$$V_{1} = \sqrt{\sigma^{2} \mu K (1 + \sqrt{1 - \Delta^{2}})}$$

$$V_{2} = \sqrt{\sigma^{2} \mu K (1 - \sqrt{1 - \Delta^{2}})}$$
(13)

where K represents the ratio of the average power of the specular components to the power of the remaining scattered components, and is given by:

$$K = \frac{V_1^2 + V_2^2 + \sum_i^{\mu} U_i^2}{2\sigma^2 \mu} \tag{14}$$

The parameter $\Delta \in [0,1]$ quantifies the similarity between the average received powers of the dominant components in cluster 1 and the power allocation to the specular components of the remaining clusters:

$$\Delta = \frac{2V_1 V_2}{V_1^2 + V_2^2 + \sum_{i}^{\mu} U_i^2} \tag{15}$$

The variables Z_i in (11) follow a Rayleigh distribution with the parameter σ defined as:

$$\sigma = \sqrt{\frac{1}{\sqrt{2\mu(1+K)}}}. (16)$$

Hence, based on (11) and using (9), and introducing delays the channel can be expressed as:

$$H_{MFTR}(z;t) = \left(\sqrt{\zeta}V_1e^{j\phi_1} + \sqrt{\zeta}V_2e^{j\phi_2} + Z_1\right)z^{-\tau_1 f_s} + \sum_{i}^{\mu} \left(\sqrt{\zeta}U_ie^{j\varphi_i} + Z_i\right)z^{-\tau_i f_s}$$

$$(17)$$

with $\tau_i \sim \mathcal{HN}(0,\sigma_\tau)$, where \mathcal{HN} denotes the half-normal distribution..

4. PROPOSED EXTENSION OF THE MULTI-CLUSTER FLUCTUATING TWO-RAY FADING MODEL

While the MFTR fading model captures clustered multipath and fluctuating line-of-sight conditions, it remains insufficient for maritime scenarios, where time-varying sea surface reflections, vessel-induced shadowing, and long-delay components with associated power loss are prominent. To address these limitations, we propose an extended model that incorporates baseband representation, Doppler effects, and stochastic differential equations (SDEs) for time-varying parameters. The baseband formulation offers a tractable framework for complex envelope analysis; Doppler shifts capture relative motion dynamics; and SDEs introduce realistic temporal evolution. Additionally, modeling associated power allows delay-dependent attenuation to be tracked, reflecting physical path loss over extended multipath trajectories.

4.1 Baseband & Doppler Shift effects

The previous model did not incorporate the carrier frequency of the signal or the effects of Doppler shifts. These factors can be integrated into the model, leading to the following updated formulation:

$$H(z;t) = \left(\sqrt{\zeta}V_1 e^{j(\phi_1 - \omega_c \tau_1 + \omega_{d_1} t)} + \sqrt{\zeta}V_2 e^{j(\phi_2 - \omega_c \tau_1 + \omega_{d_2} t)} + Z_1\right) z^{-\tau_1 f_s}$$

$$+ \sum_{i}^{\mu} \left(\sqrt{\zeta}U_i e^{j(\varphi_i - \omega_c \tau_i + \omega_{d_i} t)} + Z_i\right) z^{-\tau_i f_s}$$

$$(18)$$

 $_{
m where}$

$$Z_i = \sigma \sqrt{X_i^2 + Y_i^2} e^{-j(\varphi_{z_i} - \omega_c \tau_i + \omega_{d_i} t)}, \ i = \{1, \dots, \mu\} \ (19)$$

and $\omega_c = 2\pi f_c$, $\omega_{d_i} = 2\pi f_{d_i}$, with f_c the carrier frequency and f_{d_i} the Doppler frequency of the i^{th} cluster.

4.2 Time dependency of channel parameters

The parameters in wireless communication channels are inherently time-varying (Feng et al., 2007; Olama et al., 2009; Mossberg and Irshad, 2009). Consequently, Stochastic Differential Equations (SDEs) are employed to characterize their temporal variations and to accurately model their statistical distributions.

Following the formulation in (Mossberg and Irshad, 2009) the phase increment for the i^{th} cluster is defined as:

$$d\phi_i(t) = \sqrt{C_i^{\phi}} dW_i^{\phi}(t) \tag{20}$$

where C_i^{ϕ} denotes the variance of the process and $dW_i^{\phi}(t)$ is the increment of the Wiener process $W_i^{\phi}(t)$. The Wiener processes of the phase increments are assumed to be independent.

The time dependency of the delays is modeled as:

$$d\tau_i(t) = -\tau_i(t)dt + \sqrt{2C_i^{\tau}}dW_i^{\tau}(t)$$
 s.t $\tau_i(t) \geq 0$ (21) with C_i^{τ} the variance and $dW_i^{\tau}(t)$ the increment of the Wiener process $W_i^{\tau}(t)$. The same independence assumption as for the phase processes is applied to the Wiener processes associated with the delays.

The Rayleigh-distributed amplitude is defined as:

$$\alpha_i(t) = \sigma \sqrt{X_i(t)^2 + Y_i(t)^2} \tag{22}$$

where $X_i(t), Y_i(t)$ are designed to approximate a normal distribution. Their increment are given by:

$$dX_i(t) = -X_i(t)dt + \sqrt{2}dW_i^X(t)$$

$$dY_i(t) = -Y_i(t)dt + \sqrt{2}dW_i^Y(t)$$
(23)

where $dW_i^X(t)$ and $dW_i^Y(t)$ are the increments of the corresponding Wiener processes, which are also assumed to be independent. Consequently, the multipath components are expressed as:

$$Z_i(t) = \alpha_i(t)e^{j(\phi_i(t) - \omega_c \tau_i(t) + \omega_d t)}. \tag{24}$$

Regarding the shadowing component, the unit-mean Γ distribution is approximated using the Cox-Ingersoll-Ross

model in order to introduce realistic temporal dynamics into the shadowing process:

$$d\zeta(t) = m(1 - \zeta(t))dt + \sqrt{2|\zeta(t)|}dW^{\zeta}(t)$$
 (25)

where $dW^{\zeta}(t)$ is the increment of the Wiener process $W^{\zeta}(t)$. Finally, the variables and their increments are represented in vector form as:

$$\Lambda(t) = \begin{bmatrix}
\zeta(t) \\
\phi_1(t) \\
\phi_2(t) \\
\tau_1(t) \\
X_i(t) \\
Y_i(t) \\
\varphi_i(t) \\
\tau_i(t)
\end{bmatrix}, \quad d\Lambda(t) = \begin{bmatrix}
d\zeta(t) \\
d\phi_1(t) \\
d\phi_2(t) \\
d\tau_1(t) \\
[dX_i(t) \\
dY_i(t) \\
d\varphi_i(t) \\
d\varphi_i(t) \\
d\tau_i(t)
\end{bmatrix}$$
(26)

4.3 Physics Considerations

Several physical considerations are incorporated to enhance the accuracy of the model. Firstly, a longer delay corresponds to a greater traveled distance for the associated cluster. Consequently, a power loss is introduced as a function of the delay. The formulation of this loss is expressed as:

$$L_i(t) = L_i(d(t), \tau_i(t)) = \left(\frac{d(t)}{d(t) + c\tau_i(t)}\right)^2 \tag{27}$$

where c is the speed of light.

Secondly, given the distance, the minimum delay is expressed as $\tau_{min}=\frac{d}{c}$ and is established as a factor for the channel. Consequently, the remaining delays represent the delay spread. Finally, the Extended Time-Varying Multi-Cluster Fluctuating Two-Ray (ETVMFTR) fading channel is formulated as:

$$H(z;t) = \sqrt{L(t)L_1(t)}z^{-\left(\tau_1 + \frac{d(t)}{c}\right)}f_s$$

$$\left(\sqrt{\zeta(t)}V_1e^{j(\phi_1(t) - \omega_c\tau_1(t) + \omega_{d_1}t)}\right)$$

$$+ \sqrt{\zeta(t)}V_2e^{j(\phi_2(t) - \omega_c\tau_1(t) + \omega_{d_2}t)} + Z_1(t)$$

$$+ \sqrt{L(t)}z^{-\frac{d(t)}{c}}f_s$$

$$\left(\sum_{i}^{\mu}\left(\sqrt{L_i(t)\zeta(t)}U_ie^{j(\varphi_i(t) - \omega_c\tau_i(t) + \omega_{d_i}t)}\right)$$

$$+ \sqrt{L_i(t)}Z_i(t)\right)z^{-\tau_i(t)}f_s$$

$$\left(\sum_{i}^{\mu}\left(\sqrt{L_i(t)\zeta(t)}U_ie^{j(\varphi_i(t) - \omega_c\tau_i(t) + \omega_{d_i}t)}\right)$$

where

$$Z_i(t) = \sigma \sqrt{X_i(t)^2 + Y_i(t)^2} e^{-j(\varphi_i(t) - \omega_c \tau_i(t) + \omega_{d_i} t)}. \quad (29)$$

To ensure consistency in the total received power across different channel realizations and to prevent unintended biases in system performance evaluation, power normalization is applied:

$$H_n(z;t) = \frac{H(z;t)}{\sqrt{V_1^2 + V_2^2 + 2\mu\sigma^2}}$$
(30)

Additionally, it is assumed that the LOS components experience a lower delay than the scattered components:

$$\tau_1 \le \{\tau\}_{\mu} \tag{31}$$

where $\{\tau\}_{\mu}$ denotes the set of μ delays.

5. SIMULATION RESULTS

In this section, the performance of the proposed channel model is analyzed through numerical simulations. The statistical properties of the modeled channel, including delay spread, Doppler effects, and power variations, are examined to validate its accuracy. Further, the impact of key parameters on channel behavior is evaluated to demonstrate the model's reliability in realistic wireless communication scenarios.

Firstly, the statistical behavior of the different parameters is analyzed using quantiles, the correlation factor (R^2) and the Mean-Square Error (MSE) are presented in the Table 1:

Table 1. Quantile-based variable correlation to predefined distribution.

Variable	R^2	MSE
ζ	0.9993	$9.9962e^{-5}$
X	0.9993	$8.5040e^{-4}$
Y	0.9992	$9.2193e^{-4}$
$ au_i$	0.9987	$4.7114e^{-16}$
Z	0.9998	$1.6018e^{-5}$

where τ_i now follows a Weibull distribution due to the non-negativity of the propagation delays, as the absolute value operation guarantees physically meaningful, strictly positive delay values, and τ_1 does not follow any specific distribution since it is the minimum of $\mu+1$ SDE. The comparisons of the quantiles to their respective theoretical distributions for |Z| and ζ are presented in Fig.1 and Fig.2, respectively, thereby illustrating their closeness to the expected distributions.

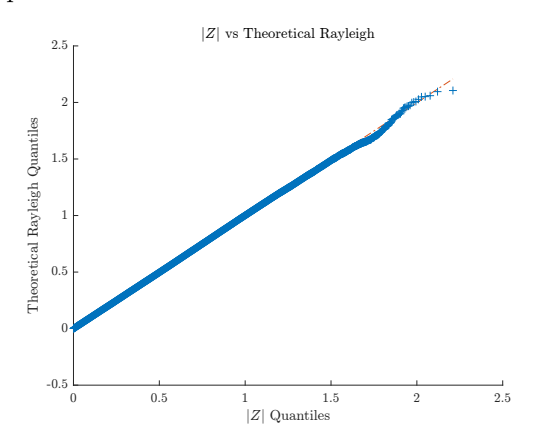


Fig. 1. |Z| quantiles comparison to Rayleigh Distribution theoretical quantiles.

The evolution of the channel over distance and time is simulated under the assumption of perfect channel knowledge and the application of a zero-forcing equalizer. A Quadrature Amplitude Modulation (QAM) 16 scheme and an Orthogonal frequency-division multiplexing (OFDM) system with 1024 subcarriers and 1024/16 guard bands are used. The simulation utilizes the parameters listed in Table 2 where G_r, G_t are the antenna receiver and transmitter gains, P_t is the transmitted power, P_w is the noise power and v is the speed of the ship. To simplify the simulation, all components are assumed to share the same Doppler frequency and variance.

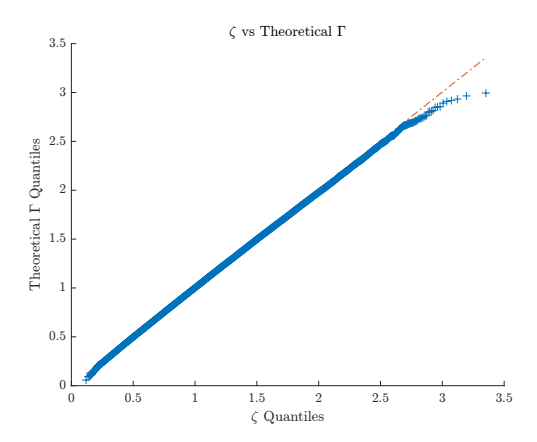


Fig. 2. ζ quantiles comparison to Γ Distribution theoretical quantiles.

Table 2. Simulation parameters.

Variables	Value	
K, Δ, μ, m	10.788, 0.29, 40, 90.252	
$C_{\phi}, C_{ au}$	$2\pi, 1e^{-10}$	
f_c, f_d, f_s	5 GHz, 100 Hz, 20 MHz	
T_c	10 ms	
G_r, G_t	0 dB, 0 dB	
P_t, P_w	40 dBm, -100 dBm	
h_t, h_r, h_e	8 m, 15 m, 35 m	
v, d_0	25 km/h, 200 m	

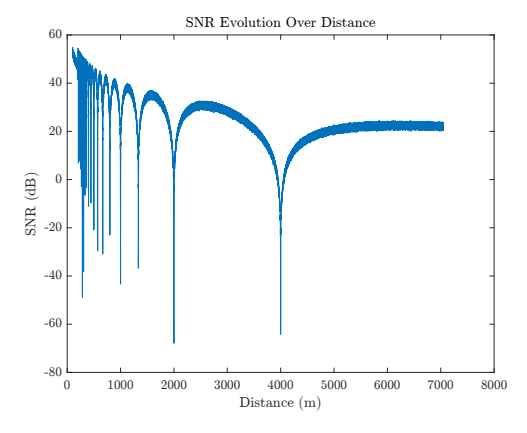


Fig. 3. SNR evolution over distance for the parameters given in Table 2.

The evolution of the Signal-to-Noise Ratio (SNR) across distance is illustrated in Fig. 3. It can be observed that the channel may enter a deep fading state depending on the distance, especially when two or three LOS components are in phase opposition. Additionally, small-scale fading introduces an envelope over large-scale fading variations. As a result, the Bit-Error Ratio (BER) fluctuates accordingly, as shown in Fig. 4. In the case of deep fading, the channel becomes unusable due to a very low SNR, resulting in a significantly high BER. The PDF of the simulated channel is illustrated in Fig. 5. The PDF aligns well with the measured LOS data presented in Fig. 5a of (Sánchez et al., 2024). A similar analysis can be performed using different macro-parameters K, Δ, μ and m. Figures 6, 7, and 8 illustrate that degraded channel conditions are being experienced, leading to a reduction in average SNR and an increased frequency of instances where the channel becomes unusable. As previously observed, the probability

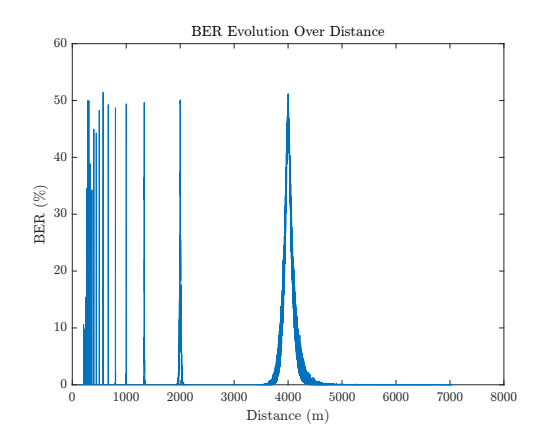


Fig. 4. BER evolution over distance for the parameters given in Table 2.

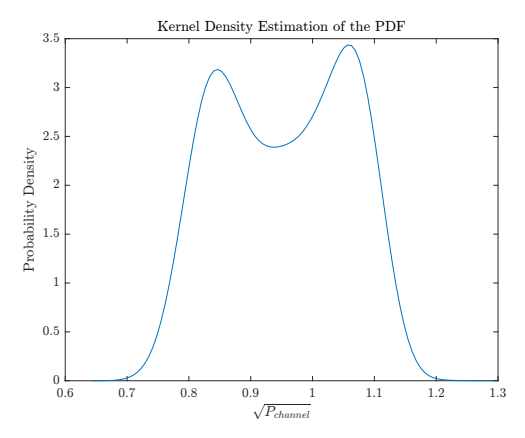


Fig. 5. Empirical PDF for the parameters given in table 2. density function is in close agreement with the measured LOS conditions reported in Fig. 5b of (Sánchez et al., 2024).

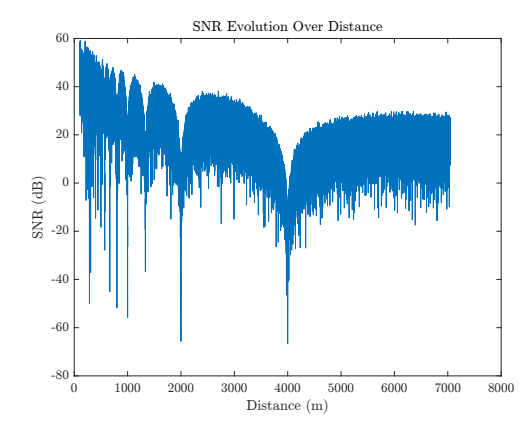


Fig. 6. SNR evolution over distance for the parameters given in Table 2 with $K=4.225, \Delta=0.999, \mu=1, m=38.868$.

6. CONCLUSIONS AND FUTURE WORK

This work presented an extended multi-cluster two-ray fading model that describes communication channels in maritime operation. The integration of a baseband model, a description of Doppler shifts, and the inclusion of Stochastic Differential Equations (SDEs) for handling time-varying parameters allowed for an improved model

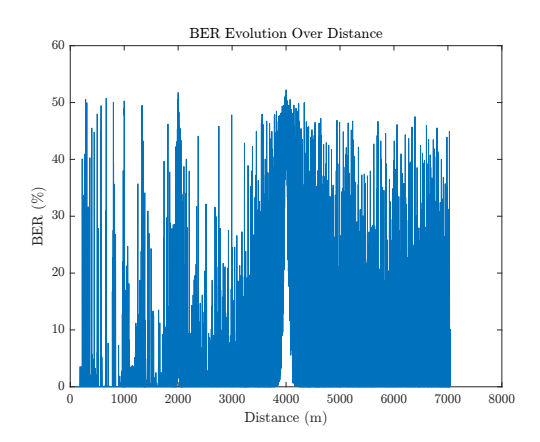


Fig. 7. BER evolution over distance for the parameters given in Table 2 with $K=4.225, \Delta=0.999, \mu=1, m=38.868$.

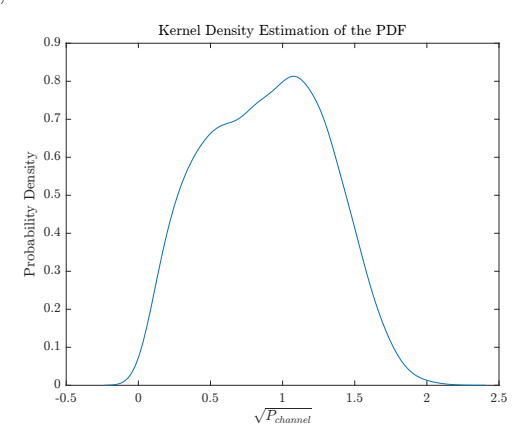


Fig. 8. Empirical PDF for the parameters given in Table 2 with $K=4.225, \Delta=0.999, \mu=1, m=38.868$.

accuracy. Numerical simulations validated the theoretical findings. Future work includes deriving distance-dependent estimation laws for K,Δ and μ incorporating transmitter height dynamics, and experimentally validating the proposed model.

ACKNOWLEDGMENTS

This research was conducted at DTU Electro as part of the SLGreen project. Shipping Lab and SLGreen is partly founded by Innovation Fund Denmark (IFD) under File No. 8090-00063B and by Danish Maritime Fund, Lauritzen Fonden, Orient's Fond and DS Norden. The authors appreciate their support.

REFERENCES

Coker, A., Straatemeier, L., Rogers, T., Valdez, P., Cooksey, D., and Griendling, K. (2013). Maritime channel modeling and simulation for efficient wideband communications between autonomous Unmanned Surface Vehicles. In 2013 OCEANS - San Diego, 1–9. doi: 10.23919/OCEANS.2013.6741084.

Eggers, P.C., Angjelichinoski, M., and Popovski, P. (2019). Wireless channel modeling perspectives for ultra-reliable communications. *IEEE Transactions on Wireless Communications*, 18(4), 2229–2243. Ekman, T. (2024). Fading Distribution Model for the

Ekman, T. (2024). Fading Distribution Model for the Maritime Radio Channel. In 2024 18th European Conference on Antennas and Propagation (EuCAP), 1–5. doi:10.23919/EuCAP60739.2024.10501319.

Feng, T., Field, T.R., and Haykin, S. (2007). Stochastic Differential Equation Theory Applied to Wireless Channels. *IEEE Transactions on Communications*, 55(8), 1478–1483. doi:10.1109/TCOMM.2007.902531.

Habib, A. and Moh, S. (2019). Wireless Channel Models for Over-the-Sea Communication: A Comparative Study. Applied Sciences, 9(3), 443. doi: 10.3390/app9030443.

Hemadeh, I.A., Satyanarayana, K., El-Hajjar, M., and Hanzo, L. (2018). Millimeter-Wave Communications: Physical Channel Models, Design Considerations, Antenna Constructions, and Link-Budget. *IEEE Communications Surveys & Tutorials*, 20(2), 870–913. doi: 10.1109/COMST.2017.2783541.

Lee, Y.H., Dong, F., and Meng, Y.S. (2014). Near Sea-Surface Mobile Radiowave Propagation at 5 GHz: Measurements and Modeling.

Marins, T.R.R., Dos Anjos, A.A., Da Silva, C.R.N., Peñarrocha, V.M.R., Rubio, L., Reig, J., De Souza, R.A.A., and Yacoub, M.D. (2021). Fading evaluation in standardized 5g millimeter-wave band. *IEEE Access*, 9, 67268–67280.

Moreno-Pozas, L., Lopez-Martinez, F.J., Paris, J.F., and Martos-Naya, E. (2016). The $\kappa - \mu$ shadowed fading model: Unifying the $\kappa - \mu$ and $\eta - \mu$ distributions. *IEEE Transactions on Vehicular Technology*, 65(12), 9630–9641.

Mossberg, M. and Irshad, Y. (2009). A Stochastic Differential Equation for Wireless Channels Based on Jakes' Model with Time-Varying Phases. In 2009 IEEE 13th Digital Signal Processing Workshop and 5th IEEE Signal Processing Education Workshop, 602–605. doi: 10.1109/DSP.2009.4785994.

Olama, M.M., Djouadi, S.M., and Charalambous, C.D. (2009). Stochastic differential equations for modeling, estimation and identification of mobile-to-mobile communication channels. *IEEE Transactions on Wireless Communications*, 8(4), 1754–1763. doi: 10.1109/TWC.2009.071068.

Romero-Jerez, J.M., Lopez-Martinez, F.J., Paris, J.F., and Goldsmith, A. (2016). The Fluctuating Two-Ray Fading Model for mmWave Communications. In 2016 IEEE Globecom Workshops (GC Wkshps), 1–6. doi: 10.1109/GLOCOMW.2016.7849062.

Romero-Jerez, J.M., Lopez-Martinez, F.J., Paris, J.F., and Goldsmith, A.J. (2017). The Fluctuating Two-Ray Fading Model: Statistical Characterization and Performance Analysis. *IEEE Transactions on Wireless Communications*, 16(7), 4420–4432. doi: 10.1109/TWC.2017.2698445.

Sánchez, J.D.V., Lopez-Martinez, F.J., Paris, J.F., and Romero-Jerez, J.M. (2024). The Multi-Cluster Fluctuating Two-Ray Fading Model. *IEEE Transactions* on Wireless Communications, 23(5), 4199–4213. doi: 10.1109/TWC.2023.3315732.

Tse, D. and Viswanath, P. (2005). Fundamentals of wireless communication. Cambridge university press.

Wang, J., Zhou, H., Li, Y., Sun, Q., Wu, Y., Jin, S., Quek, T.Q.S., and Xu, C. (2018). Wireless Channel Models for Maritime Communications. *IEEE Access*, 6, 68070–68088. doi:10.1109/ACCESS.2018.2879902.